# Fast evaluation of local elastic constants and its application to nanosized structures

Zhiwei Cui, Shaorui Yang, and L. Catherine Brinson

Phys. Rev. B **91**, 184104 — Published 6 May 2015

DOI: 10.1103/PhysRevB.91.184104

# Fast Evaluation of Local Elastic Constants and its Application to nano-sized Structures

Zhiwei Cui, Shaorui Yang, L. Catherine Brinson*

Department of Mechanical Engineering

Northwestern University

Evanston, IL, 60208, USA

* Corresponding author. Email address: cbrinson@northwestern.edu; Phone: 847-467-2347

**Abstract**

We derive a method to determine the effective local elasticity tensor by combining the local stress, local strain, and global strain in conjunction with a linear least square solver. This method reduces to the standard stress-strain fluctuation method for the estimation of global moduli if the local stress and the local strain are substituted by global counterparts. The quality of the developed method is verified by the analysis of an FCC Lennard-Jones single crystal. By using this method, surface elastic behaviors of three nano-plates are investigated. Simulation results prove that both softening and stiffening effects could be detected, depending on the surface orientations and loading directions. This novel approach could be especially valuable for complicated morphologies where the physical properties of the local material are challenging or impractical to obtain.

**Keywords:** local elastic constants; linear least square solver; molecular dynamics simulations;

## 1. Introduction

In recent years, nano-composites have gained increasing attention in both academic and industrial research with diverse applications. The overall performances of these materials are superior to the simple superposition of the properties of their individual constituents [1-3]. In polymer based nano-composites, a polymer region around the nanoparticle, where the material properties deviate from the bulk behavior, has been confirmed experimentally [4-6]. This local region is known as the interphase and arises from intertwined chemical interactions and geometrical constraints. How to characterize the material properties, especially mechanical performances, within the interphase region are of significant theoretical, experimental, and industrial interest. Nano-composites are clearly spatially and mechanically inhomogeneous at nanometer length scales. Similar heterogeneity has also been observed in amorphous glassy materials, which are traditionally treated as a mechanically homogeneous continuum. The local heterogeneity in the elastic properties is acknowledged and ascribed to the localized structural rearrangements [7-9]. Indeed, heterogeneity and homogeneity are strongly dependent on the length scales used in the observation [10]. At a specific length scale, some constituents in a given material are identifiable to be homogeneous, but may become heterogeneous while observed at a smaller length scale. Therefore there is a critical need to develop methodologies to investigate the local material properties. These local property data can provide new insights that will enable the tailoring of the microstructure to optimize their performances and provide a better understanding that reflect microstructural composition on the macroscopic observable properties. In theory, these local properties could be measured experimentally. In reality, the complex morphology of these systems has prevented facile determination of them.

With recent advances in computational algorithms and computer hardware, atomistic level computations, such as molecular dynamic (MD) simulation and Monte Carlo method, have

become effective and efficient tools for simulating material behavior and for computing material properties [11-13]. To compute the *global* elastic constants by atomic simulations, two fundamentally different approaches, the deformation-based and the fluctuation-based methods, have been widely applied. From the viewpoint of the continuum mechanics, one can simply obtain the elastic constants through the linear dependence between the resultant stresses and applied small strains. This is known as the deformation-based approach [14]. Nevertheless, this technique suffers from the fluctuations in stresses and strains at a non-zero temperature, and is only valid for a static/quasi-static condition, i.e., around 0K. At a finite temperature, fluctuation methods are always employed [15]. In a seminal paper, Parrinello and Rahman (PR) developed the strain fluctuation formula to compute the isothermal elastic constant tensor in isothermal-isobaric (NPT) ensemble [16]. However, this method was found to converge slowly for many systems. Subsequently, the stress-strain fluctuation formula was explored based on statistical thermodynamics with much better convergence [17, 18]. The estimation of elastic constants is dependent on both strain and stress, not only strain itself as in PR method. The essence of its rapid convergence is manifested via a linear least square solver [19].

To obtain the *local* elastic modulus, one can follow the same methodologies mentioned above with the change from global stresses and strains into local stresses and strains. For the deformation-based technique [20], Mizuno et al compared with three different approaches by using the same glassy materials [7, 21]. In order to suppress the fluctuation of stresses and strains, the simulation temperature is extremely low. Other significant efforts have also been devoted to obtain the local elastic constants through the stress-fluctuation method [7, 8, 22-26], where the local material is hypothesized to undergo the deformation with the global strains. Under such an assumption, the local elasticity tensor is obtained directly through the local stress and global strain, resulting in an approximation to the true local elastic constants.

In this paper, we present a novel method for the estimation of the *local* elasticity tensor, combining the information of global strain, local stress, and local strain. This new approach is applicable to all the local regions by a single simulation with rapid convergence. It is shown that our new formula reduces to the stress-strain fluctuation technique [18, 19] if the local strain and local stress are substituted by global ones. For simplicity, a FCC crystal structure is studied to verify the developed algorithm and to compare with these formulae. No polymers are considered in the current work.

To illustrate the application of the newly developed method, three Lennard-Jones FCC crystals with free surfaces on $\{100\}$, $\{110\}$, and $\{111\}$ are investigated. The Young's moduli distributions are calculated in parallel with and perpendicular to the free surface. Both stiffening and softening effects are observed, depending on the surface orientations.

## 2. Methodology

In terms of the macroscopic average theory [10], the average stress and strain over a domain $\Omega$ are

$$\overline{\boldsymbol{\sigma}} = \frac{1}{\Omega}\int_{\Omega} \boldsymbol{\sigma} dV \quad , \quad \overline{\boldsymbol{\varepsilon}} = \frac{1}{\Omega}\int_{\Omega} \boldsymbol{\varepsilon} dV \quad , \tag{1}$$

where $\boldsymbol{\sigma}$ and $\boldsymbol{\varepsilon}$ are the stress and strain at $dV$, respectively. Note that the domain $\Omega$ could be heterogeneous and may contain more than one inhomogeneity. A straightforward definition of the effective modulus (stiffness) tensor of the heterogeneous material can be found from the following relationship

$$\overline{\boldsymbol{\sigma}} = \overline{\mathbf{C}}\,\overline{\boldsymbol{\varepsilon}} \quad , \tag{2}$$

where $\overline{\boldsymbol{\sigma}}$ and $\overline{\boldsymbol{\varepsilon}}$ are, respectively, the average stress and strain tensors, and the fourth tensor $\overline{\mathbf{C}}$ defined by (2) is called the *effective modulus* tensor of the heterogeneous material.

Consider a composite material with $N$ inhomogeneities, the average strain and stress of the

entire material could be written as

$$\overline{\boldsymbol{\sigma}} = \sum_{r=0}^{N} c_r \overline{\boldsymbol{\sigma}}_r \quad , \quad \overline{\boldsymbol{\varepsilon}} = \sum_{r=0}^{N} c_r \overline{\boldsymbol{\varepsilon}}_r \quad , \tag{3}$$

where $\overline{\boldsymbol{\sigma}}_r$ and $\overline{\boldsymbol{\varepsilon}}_r$ are the average stress and strain of the $r$ th inhomogeneity, and $c_r$ is the volume fraction of the $r$ th inhomogeneity and $r = 0$ denotes the matrix. For convenience, we introduce three distinct modulus tensors. The first one is the *effective global elasticity tensor*, as expressed in Eq. (2), which correlates the global strain and global stress of the entire composite. The second one is called the *effective local modulus tensor*. For example, the local elasticity tensor of the $r$ th inhomogeneity can be obtained through [10]

$$\overline{\boldsymbol{\sigma}}_r = \overline{\mathbf{C}}_r \, \overline{\boldsymbol{\varepsilon}}_r \quad . \tag{4}$$

It should be noted that such a relationship differs from those defined in Refs. [7, 27], since we adopt the local stress and local strain to define the local modulus. Suppose all the inhomogeneities possess the global average strain, the linear mapping between the local stress and global strain is known as the *effective intermediate modulus tensor*, i.e.,

$$\overline{\boldsymbol{\sigma}}_r = \overline{\mathbf{C}}_{rs} \, \overline{\boldsymbol{\varepsilon}} \quad . \tag{5}$$

This modulus provides a way to link the applied loading on the composite to local response, which has been widely described as the 'local' modulus in the open literatures [7, 27]. However, based on traditional micromechanics [10], $\overline{\mathbf{C}}_r$ from Eq. (4) is a better definition of the true local modulus. Note that a similar intermediate modulus has been reported to study the role of the partial potential on the mechanical properties [28]. From Eqs. (2), (3), and (5), we have

$$\overline{\mathbf{C}} = \sum_{r=0}^{N} c_r \overline{\mathbf{C}}_{rs} \quad , \tag{6}$$

suggesting that the global elasticity tensor could be fully recovered after averaging the intermediate modulus.

Note that $\overline{\boldsymbol{\sigma}}$ and $\overline{\boldsymbol{\varepsilon}}$ are the average stress and strain of the entire composite material while

$\bar{\boldsymbol{\sigma}}_r$ and $\bar{\boldsymbol{\varepsilon}}_r$ are the average stress and strain of the $r$ th inhomogeneity. We can utilize the stress concentration tensor ( $\mathbf{A}_r$ ) and strain concentration tensor ( $\mathbf{B}_r$ ), i.e.,

$$\bar{\boldsymbol{\sigma}}_r = \mathbf{A}_r \bar{\boldsymbol{\sigma}} \quad , \quad \bar{\boldsymbol{\varepsilon}}_r = \mathbf{B}_r \bar{\boldsymbol{\varepsilon}} \quad . \tag{7}$$

Combined with Eqs. (2)~(7), we can obtain the following expression

$$\bar{\mathbf{C}}_r = \mathbf{A}_r \bar{\mathbf{C}} \mathbf{B}_r^{-1} = \bar{\mathbf{C}}_{rs} \mathbf{B}_r^{-1} \quad . \tag{8}$$

Apparently, the three moduli are not independent and can be converted into each other with the aid of the concentration tensors. For instance, the local elasticity tensor can be evaluated directly if the global modulus and two concentration tensors are known, which requires all the information of the global and local stresses and strains. On the other hand, many approaches have been presented to predict the intermediate modulus in NVT ensemble, where the shape and volume of the simulation system is fixed, i.e., no global strain. Consequently, their methods are limited to the local modulus estimation since the strain concentration tensor defined in Eq. (7) cannot be assessed.

As described above, Eq. (8) provides two techniques that could be used to determine the local elastic constants. One requires the evaluation of the global elasticity and two concentration tensors while the other needs the intermediate modulus and strain concentration tensor. Below, we will discuss each term in detail.

In Refs [18, 19], the stress-strain fluctuation formula is used to estimate the adiabatic and isothermal elastic constants in NPH and NPT ensembles, respectively. In that method, the global elastic constants are computed through

$$\bar{C}_{ijkl} = \left\langle \bar{\sigma}_{ij} \, \bar{\varepsilon}_{mn} \right\rangle \left\langle \bar{\varepsilon}_{mn} \, \bar{\varepsilon}_{kl} \right\rangle^{-1} \tag{9}$$

where the bracket $\langle \ \rangle$ denote the ensemble average. The global stress $\bar{\sigma}_{ij}$ and global strain $\bar{\varepsilon}_{ij}$ of a given simulation system are given by

$$\bar{\sigma}_{ij} = -\frac{1}{V}\left[\sum_{\alpha} m_{\alpha}\left(v_{\alpha}\right)_{i}\left(v_{\alpha}\right)_{j} - \sum_{\beta>\alpha}\frac{\partial U}{\partial r_{\alpha\beta}}\frac{\left(r_{\alpha\beta}\right)_{i}\left(r_{\alpha\beta}\right)_{j}}{r_{\alpha\beta}}\right] , \tag{10}$$

$$\bar{\varepsilon}_{ij} = \frac{1}{2}\left[\left\langle h\right\rangle_{ik}^{-T} h_{kl}^{T} h_{lm} \left\langle h\right\rangle_{mj}^{-1} - \delta_{ij}\right] , \tag{11}$$

where $V$ is the volume of the system. $m_{\alpha}$ and $v_{\alpha}$ are the mass and velocity of the $\alpha$ th atom, respectively. $U$ is the potential energy and assumed as a function of atomic distance. $r_{\alpha\beta}$ is the distance between the atoms indexed as $\alpha$ and $\beta$. $h$ is the scaling matrix $h=\left\{\vec{a},\vec{b},\vec{c}\right\}$, where $\vec{a}$, $\vec{b}$, and $\vec{c}$ are three basis vectors describing the size and shape of the simulation box. The matrix $\left\langle h\right\rangle$ is the average frame of the system as the reference state. $h^{-T}$ is the inverse of the transpose of $h$, and $\delta_{ij}$ is the Kronecker tensor. In this paper, Latin indices $i,j,k,l,m,n$ represent the Cartesian coordinates in three dimensions and run from 1 to 3. Greek indices refer to particle labels. The conventional suffix notation is used, where repeated suffixes indicate summation over the values of 1, 2, 3 unless otherwise stated.

In order to estimate the stress and strain concentration tensors, we need to calculate the local stress and local strain tensors. Without loss of generality, every atom could be recognized as an inhomogeneity, indicating those local variables are the averaging effect over all the atoms in the local region. We thus consider per-atom stress and per-atom strain tensors. Based on the assumption of equal portions from each atom, the per-atom stress could be defined as [29, 30],

$$\left(\sigma_{\alpha}\right)_{ij} = -\frac{1}{V_{\alpha}}\left[k_{B}T\delta_{ij} + \sum_{m} k_{m}\left(r_{\alpha}\right)_{i}\left(f_{\alpha}\right)_{i}\right] , \tag{12}$$

where $V_{\alpha}$ is the atomic volume. $k_{B}$ is the Boltzmann constant, and $T$ is the temperature. $k_{m}$ is the weighting factor, and should be $1/2$ for pairwise non-bond potential and bond potential, $1/3$ for angle potential, $1/4$ for dihedral potential, and so forth. Since it is a symmetric tensor for each atom, only 6 independent components will be stored. The individual atomic volume is

not readily defined or measured, especially in the deformed state. In this work, a Voronoi tessellation is used to approximate the volume for each atom. Note that the global stress defined in Eq. (10) can be recovered by averaging the atomic stress from Eq. (12).

For the per-atom strain, we first need to define a reference configuration, where each atom locates its equilibrium position. This could be achieved by averaging the atomic coordinates after a sufficiently long simulation. At each step, the atomic deformation gradient matrix $\mathbf{J}_\alpha$ of the $\alpha$ th atom can be obtained through [31, 32]

$$\left(r_{\alpha\beta}\right)_i = \left(J_\alpha\right)_{ij} \left\langle r_{\alpha\beta} \right\rangle_j \quad . \tag{13}$$

The $\left\langle \mathbf{r}_{\alpha\beta} \right\rangle$ denotes the average interatomic distance in the reference state. Within the cutoff distance, we seek the optimal $\mathbf{J}_\alpha$ to satisfy the criterion above for all the neighbor atoms of the $\alpha$ th atom at the reference configuration, indicating

$$\Pi_\alpha = \sum_\beta \left| \left(r_{\alpha\beta}\right)_i - \left(J_\alpha\right)_{ij} \left\langle r_{\alpha\beta} \right\rangle_j \right|^2 \quad , \quad \Pi_\alpha \to 0 \quad . \tag{14}$$

This leads to

$$\left(J_\alpha\right)_{ij} = \left\{ \sum_\beta \left[ \left(r_{\alpha\beta}\right)_i \left\langle r_{\alpha\beta} \right\rangle_k \right] \right\} \left\{ \sum_\beta \left[ \left\langle r_{\alpha\beta} \right\rangle_k \left\langle r_{\alpha\beta} \right\rangle_j \right] \right\}^{-1} \quad . \tag{15}$$

Then the atomic strain tensor is

$$\left(\varepsilon_\alpha\right)_{ij} = \frac{1}{2} \left[ \left(J_\alpha\right)^T_{ik} \left(J_\alpha\right)_{kj} - \delta_{ij} \right] \quad . \tag{16}$$

With such per-atom variables, the local stress and local strain tensors could be obtained for the $r$ th local domain, i.e.,

$$\left(\bar{\sigma}_r\right)_{ij} = \sum_{\alpha \in r} \frac{V_\alpha}{V_r} \left(\sigma_\alpha\right)_{ij} \quad , \quad \left(\bar{\varepsilon}_r\right)_{ij} = \sum_{\alpha \in r} \frac{V_\alpha}{V_r} \left(\varepsilon_\alpha\right)_{ij} \quad , \tag{17}$$

where $V_\alpha / V_r$ is the volume fraction of the $\alpha$ th atom. According to Eqs. (3), (6), (9), and (17), we can have the formula for the estimation of the intermediate modulus tensor immediately

$$\left(\bar{C}_{rs}\right)_{ijkl} = \left\langle \left(\bar{\sigma}_r\right)_{ij} \bar{\varepsilon}_{mn} \right\rangle \left\langle \bar{\varepsilon}_{mn} \bar{\varepsilon}_{kl} \right\rangle^{-1} \quad . \tag{18}$$

The local strain and global strain is connected through the strain concentration tensor, as expressed in Eq. (7), i.e.,

$$\left(\bar{\varepsilon}_r\right)_{ij} = \left(B_r\right)_{ijkl} \bar{\varepsilon}_{kl} \quad . \tag{19}$$

Such a function, however, cannot be satisfied exactly in each step. After the simulation, $n$ pairs of the local and global strains are obtained. The difference between them is

$$\Delta_r = \sum_{i,j} \sum_{s=1}^{n} \left| \left(\bar{\varepsilon}_r\right)_{ij}^{s} - \left(B_r\right)_{ijkl} \bar{\varepsilon}_{kl}^{s} \right|^2 \quad . \tag{20}$$

Follow the linear least square algorithm [19], the function $\Delta_r$ reaches minimum once $\partial \Delta_r / \partial \left(B_r\right)_{ijkl} = 0$, yielding

$$\left(B_r\right)_{ijkl} = \left\langle \left(\bar{\varepsilon}_r\right)_{ij} \bar{\varepsilon}_{mn} \right\rangle \left\langle \bar{\varepsilon}_{mn} \bar{\varepsilon}_{kl} \right\rangle^{-1} \quad . \tag{21}$$

The stress concentration tensor can be deduced via the same procedure and is shown as follows,

$$\left(A_r\right)_{ijkl} = \left\langle \left(\bar{\sigma}_r\right)_{ij} \bar{\sigma}_{mn} \right\rangle \left\langle \bar{\sigma}_{mn} \bar{\sigma}_{kl} \right\rangle^{-1} \quad . \tag{22}$$

Since Eqs. (9)~(22) provide all the quantities in Eq. (8), the local elasticity tensor can be estimated directly in conjunction with the global elasticity, Eq. (9), and two concentration tensors, Eqs. (21), and (22), namely,

$$\left(\bar{C}_r\right)_{ijkl} = \left\langle \left(\bar{\sigma}_r\right)_{ij} \bar{\sigma}_{mn} \right\rangle \left\langle \bar{\sigma}_{mn} \bar{\sigma}_{pq} \right\rangle^{-1} \left\langle \bar{\sigma}_{pq} \bar{\varepsilon}_{uv} \right\rangle \left\langle \left(\bar{\varepsilon}_r\right)_{uv} \bar{\varepsilon}_{kl} \right\rangle^{-1} \quad . \tag{23}$$

As the second choice, one can also derive the local elasticity tensors based on the intermediate modulus, Eq. (18), and strain concentration tensors, Eq. (21), i.e.,

$$\left(\bar{C}_r\right)_{ijkl} = \left\langle \left(\bar{\sigma}_r\right)_{ij} \bar{\varepsilon}_{mn} \right\rangle \left\langle \left(\bar{\varepsilon}_r\right)_{mn} \bar{\varepsilon}_{kl} \right\rangle^{-1} \tag{24}$$

In principle, Eq. (23) and Eq. (24) should give the same results but the latter is more concise and easy to apply since the bulk stress and its derivative ($\mathbf{A}_r$) are not included. Accordingly, we adopt the formula in Eq. (24) to calculate the local elasticity tensor in the subsequent section.

It should be noted that Eq. (24) reduces to the global elasticity tensor defined in Eq. (9) if the

local stress and local strain are replaced by the global ones. However, the appearance of the local stress and local strain makes the computational formula in Eq. (24) more versatile since it can be applied for the estimation of the elasticity tensor for arbitrary size of the local material. Next, again considering one atom as an inhomogeneity, one can show the atomic elasticity tensor to be

$$(C_\alpha)_{ijkl} = \left\langle (\sigma_\alpha)_{ij}\, \bar{\varepsilon}_{mn} \right\rangle \left\langle (\varepsilon_\alpha)_{mn}\, \bar{\varepsilon}_{kl} \right\rangle^{-1} \tag{25}$$

## 3. MD Simulations

To check the validity of the aforementioned algorithms, a 10×10×10 FCC crystal structure using standard 12-6 Lennard-Jones potential is studied. The simulation system is divided into 10 thin slabs along $z$ direction, where each slab is regarded as one local region. The simulation cell contains 4000 atoms with 400 atoms in each slab. To eliminate the size effect, periodic boundary conditions are applied to three directions. All the MD simulations are conducted by using the LAMMPS software package [33, 34]. In our simulations, NPT statistical ensemble is adopted, implemented by Nose-Hoover thermostat and Parrinello-Rahman pressostat. The external pressure is fixed as 0. The velocity-Verlet algorithm is chosen to integrate the equations of motion. All the simulation systems are first equilibrated in NPT ensemble for $1\times10^7$ steps, then additional $2\times10^7$ steps are evolved to collect the results.

For Lennard-Jones potential, all the quantities can be express in a reduced unit system, where the fundamental units are $\sigma = 1$ for length, $\varepsilon = 1$ for energy, $m = 1$ for mass and $k_B = 1$ for the Boltzmann constant. Other units of interest can be derived from these fundamental units, such as temperature in $\varepsilon/k_B$, pressure in $\varepsilon/\sigma^3$, and time in $\tau = \sqrt{m\sigma^2/\varepsilon}$. Timestep is set as $0.001\tau$. The cutoff distance is $R_c = 2.5\sigma$.

For cubic crystals, there are only three independent elements of the elastic constant matrix, $C_{11}$, $C_{12}$, $C_{44}$. All the results exhibited below are the averaging data, i.e.,

$C_{11} = \left(C_{11} + C_{22} + C_{33}\right)/3$, $C_{12} = \left(C_{12} + C_{13} + C_{23}\right)/3$, and $C_{44} = \left(C_{44} + C_{55} + C_{66}\right)/3$.

Since the simulation system is a homogeneous single crystal structure, it should restore the global strain for the entire system if the local strain defined in Eq. (16) and simulation parameters are correct. In order words, the estimation of the global elasticity tensor (as shown in Eq. (9)) from two different approaches should be the same. One is calculated through the evolution of scaling matrix $h$, see Eq. (11), while the other is calculated through the per-atom strain and averages over all the atoms in the entire system. Tabulated in the Table 1 are the data calculated through two approaches. The results from atomic strain are very close to the standard algorithm, Eq. (11). Some small discrepancies between them could be ascribed to the chosen reference frame and the atomic equilibrium positions. Overall, such a good agreement establishes the validity of per-atom strain, revealing that the atomic strain captures the deformation of each atom and could be summed up to recover the global strain. This is particularly important while exploring the surface effect where the periodic boundary condition cannot be applied on the free surfaces. In that case, global strain can only be determined by using the per-atom strain due to the absence of scaling matrix $h$.

Table 1 Comparison of the global elasticity tensor between scaling matrix $h$ and per-atom strain defined in Eq. (16). The total isothermal elastic constants are in Lennard-Jones units for give temperatures. The first row at each temperature displays the results obtained through the evolution of scaling matrix $h$ while the second row is from atomic strain.

| $T$ | $C_{11}$ | $C_{12}$ | $C_{44}$ |
|---|---|---|---|
| 0.1 | 81.43 | 48.00 | 49.61 |
| | 81.38 | 47.95 | 49.61 |

| | | | |
|---|---|---|---|
| 0.2 | 70.51<br>70.43 | 41.79<br>41.71 | 44.10<br>44.09 |
| 0.3 | 61.84<br>61.74 | 36.23<br>36.13 | 39.15<br>39.14 |
| 0.4 | 53.66<br>53.49 | 31.34<br>31.16 | 34.09<br>34.08 |
| 0.5 | 44.00<br>43.79 | 25.13<br>24.91 | 29.11<br>29.11 |

The elastic constants $C_{11}$, $C_{12}$, and $C_{44}$ of each thin slab at the temperatures of 0.1 and 0.5 are portrayed in Figure 1, where the symbols are the local elastic constants and the solid lines represent the bulk behavior. Clearly, all the elastic constants from the local regions fluctuate around the global tensor with small variations. Since each thin slab is also an ideal crystal, there is no essential difference between them and the whole system, which implies that the local modulus should be identical to the bulk behavior. The maximum relative deviation is less than 1% for all the temperature range studied here, demonstrating the validity of our algorithm.

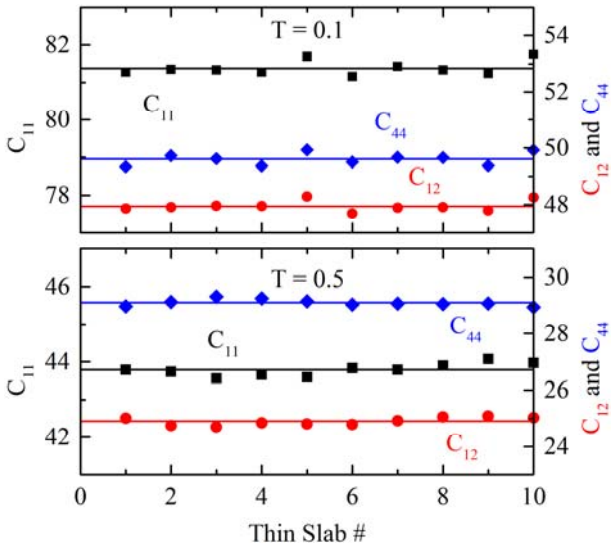


Figure 1 Comparison of local elastic constants vs. global elastic constants at a temperature of 0.1 and 0.5. Symbols are the results for local elastic constants calculated by Eq. (24), where square, circle, and diamond denote $C_{11}$, $C_{12}$ and $C_{44}$, respectively. Solid lines are the corresponding bulk behavior.

We then compare the convergence of the three main elastic constants $C_{11}$, $C_{12}$, and $C_{44}$ via Eqs. (9), (18), and (24) at the temperature of 0.5. The computation data are depicted in Figure 2. The elastic constants exhibit the same converging speed and could be assumed to be converged after $1\times10^7$ steps. In addition, negligible discrepancies between global, intermediate, and local moduli after convergence reveal that the stress and strain concentration tensors ($\mathbf{A}_r$ and $\mathbf{B}_r$) for the thin slab #5 are unit fourth order tensors according to their relationships expressed in Eq. (8). Therefore, the local (from Eqs. (23) and (24)), intermediate, and global moduli are equivalent for perfect crystals.

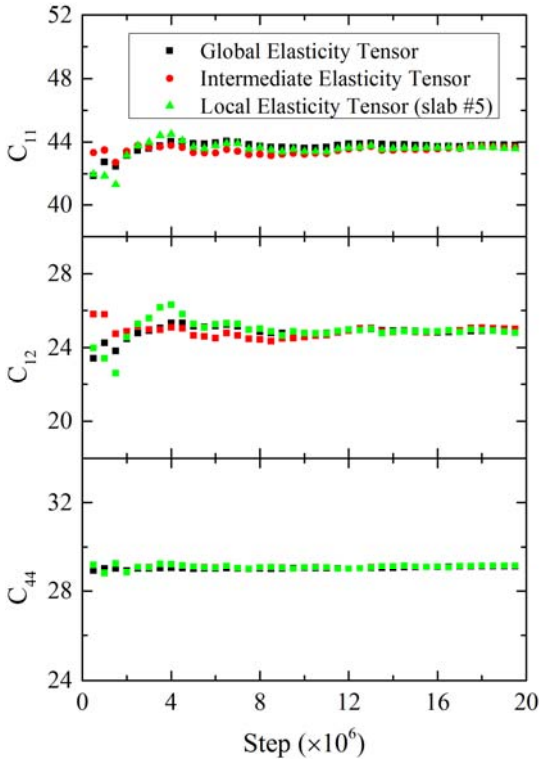


Figure 2 Convergence of local, intermediate, and global elasticity tensors for an FCC Lennard-Jones crystal at T=0.5.

As an example to illustrate the use of the newly developed method, we consider the surface effect on the local elasticity tensors. This is because the free surface plays a vital role for nano-sized structures, where the mechanical properties deviate significantly from their bulk forms because of high surface-to-volume ratios [35, 36]. To date, extensive numerical simulations [37, 38] and theoretical modeling [39-41] have been performed to investigate the size dependence of global elastic properties for entire nano-sized structures. However, limited work was focused on the local material behavior. In the current work, three Lennard-Jones FCC crystal structures with free surfaces on $\{100\}$, $\{110\}$, and $\{111\}$ are considered. A typical simulation cell of a nano-plate is shown in Figure 3. Periodic boundary conditions are applied only in the two horizontal directions, while keeping the top and the bottom of the simulation cell as free

surfaces. To fully explore the surface effect, three large systems, containing 16400 atoms (10×20×20), 16400 atoms (10×20×10), and 16000 atoms (5×10×13) for $\{100\}$, $\{110\}$, and $\{111\}$ surfaces, are studied. They have, respectively, 41, 41, and 40 atomic layers parallel to the free surfaces. All the systems are partitioned into pieces along $Z$ direction, where each piece is one atomic layer including 400 atoms. Parrinello-Rahman pressostat is applied on $X$ and $Y$ directions with 0 external pressure.

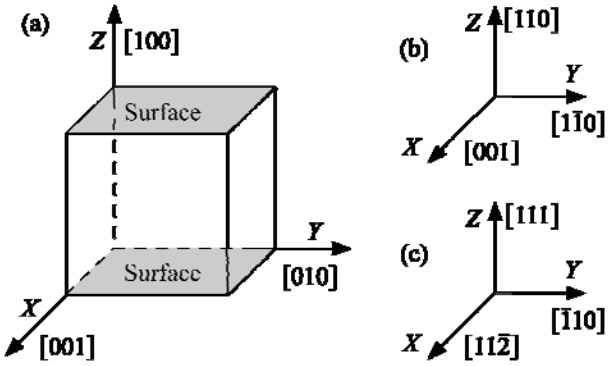


Figure 3 Schematic illustration of the simulation system used to study the surface effect of FCC Lennard-Jones crystals with three orientations. The $Z$ surface is free, while $X$ and $Y$ axes are subjected to the periodic boundary conditions. a), b), and c) illustrate three crystallographic orientations with the free surface on $\{100\}$, $\{110\}$, and $\{111\}$.

It should be noted that the Voronoi tessellation is a good approximation for the system with all periodic boundary conditions on three directions but overestimates the atomic volume on the top surface layer due to limited coordinate neighbors. Therefore in this case, we use the atomic volume estimated from the second layer as the approximation of the atomic volume in the first layer, i.e., the atomic volume and local volume of the first two layers are assumed to be the same.

Because of different orientations and surface effect, each layer now becomes an orthotropic structure. Hence there are nine independent elements in the elastic constant matrix, i.e.,

$$C=\begin{bmatrix} C_{11} & C_{12} & C_{13} & 0 & 0 & 0 \\ C_{12} & C_{22} & C_{23} & 0 & 0 & 0 \\ C_{13} & C_{23} & C_{33} & 0 & 0 & 0 \\ 0 & 0 & 0 & C_{44} & 0 & 0 \\ 0 & 0 & 0 & 0 & C_{55} & 0 \\ 0 & 0 & 0 & 0 & 0 & C_{66} \end{bmatrix}. \tag{26}$$

The corresponding compliance tensor is

$$S=C^{-1}=\begin{bmatrix} 1/E_1 & -\nu_{21}/E_2 & -\nu_{31}/E_3 & 0 & 0 & 0 \\ -\nu_{12}/E_1 & 1/E_2 & -\nu_{32}/E_3 & 0 & 0 & 0 \\ -\nu_{13}/E_1 & -\nu_{23}/E_2 & 1/E_3 & 0 & 0 & 0 \\ 0 & 0 & 0 & 1/G_{23} & 0 & 0 \\ 0 & 0 & 0 & 0 & 1/G_{13} & 0 \\ 0 & 0 & 0 & 0 & 0 & 1/G_{12} \end{bmatrix}, \tag{27}$$

including three Young's moduli ($E_1$ , $E_2$ and $E_3$), three shear moduli ($G_{12}$ , $G_{13}$ and $G_{23}$), and six Poisson's ratios ($\nu_{12}$ , $\nu_{21}$, $\nu_{13}$, $\nu_{31}$, $\nu_{23}$ and $\nu_{32}$). Note that only three Poisson's ratios are independent to hold the symmetry for the compliance tensor, so we have

$$\frac{\nu_{12}}{E_1}=\frac{\nu_{21}}{E_2}\ ,\ \frac{\nu_{13}}{E_1}=\frac{\nu_{31}}{E_3}\ ,\ \frac{\nu_{23}}{E_2}=\frac{\nu_{32}}{E_3}\ . \tag{28}$$

For each simulation system, we will consider three Young's moduli $E_1$ , $E_2$ and $E_3$ that are aligned with $X$ , $Y$ , and $Z$ directions, respectively. Clearly, $E_1$ and $E_2$ are in parallel with the free surface while $E_3$ is perpendicular to the surface. For simplicity, we add the surface as the superscript, such as, $E_1^{\{100\}}$ denotes the Young's modulus parallel to the $\{100\}$ surface along $\langle 100\rangle$ direction and $E_3^{\{111\}}$ is the Young's moduli perpendicular to the $\{111\}$ surface along $\langle 111\rangle$ direction.

The simulation results are presented in Figure 4. The symbols represent the local Young's

moduli while straight solid lines represent the corresponding bulk behavior. Several important features are observed in the results. First, two distinct regimes that denote surface and bulk states are detected along $Z$ axis. Since this is a nano-plate structure, both the bottom and the top are free surfaces and their mechanical properties are nearly the same, providing one validation our simulations. In addition, both modulus and stress profiles suggest that the effective surface zone is around 3~5 atomic layers, depending on surface directions. The intermediate regime is known as the bulk region. In fact, most of the previous atomistic simulation work considered the effective global modulus for the entire nano-structure under different external loadings [37, 42, 43]. Yet, our data display a full gradient mapping of the local modulus, revealing the mechanical heterogeneity of nano-sized structures.

A second aspect of the results is that both softening and stiffening of $E_1$ and $E_2$ are possible. The major source for such phenomena could be the uneven distribution of local average stresses, as shown in Figure 4 b). For instance, softening effect is dominant for $E_1^{\{100\}}$ because of the negative average stress at the surface layers. In other words, the surface structure $\{100\}$ undergoes a tensile deformation, indicating a softer response relative to bulk behavior. In contrast, $E_2^{\{111\}}$ displays a stiffening effect due to the surface compressive stress. Combined with the bulk behaviors of the intermediate regime, the overall mechanical performances of $E_2^{\{111\}}$ and $E_1^{\{100\}}$ are, respectively, stiffer and softer elastically than the corresponding bulk. Such a discovery agrees with the previous work on FCC Cu structure [42].

A third feature of the results is that all the moduli $E_3$ that are perpendicular to the surface drop steeply at the surface region. A zigzag shape is observed on $\{100\}$ and $\{111\}$ surfaces while the Young's modulus $E_3^{\{110\}}$ on the $\{110\}$ surface declines monotonically. Such different

phenomena are the competition outcome between the local stress, local strain and global strain. Since we cannot control the pressure in the $Z$ direction, the mechanical performances are solely determined by the microstructural change, i.e., atomic coordination. Note that the vertical Young's modulus $E_3$ at the first atomic layer is extremely small, leading to an overall softening effect along $Z$ axis, regardless of the surface orientations. The decrement of the vertical Young's modulus is in good agreement with the experimental observations for polymer systems [44]. Apparently, the above analysis and discussions for the FCC structure indicates the importance in accounting for free surface effects in calculating local moduli.

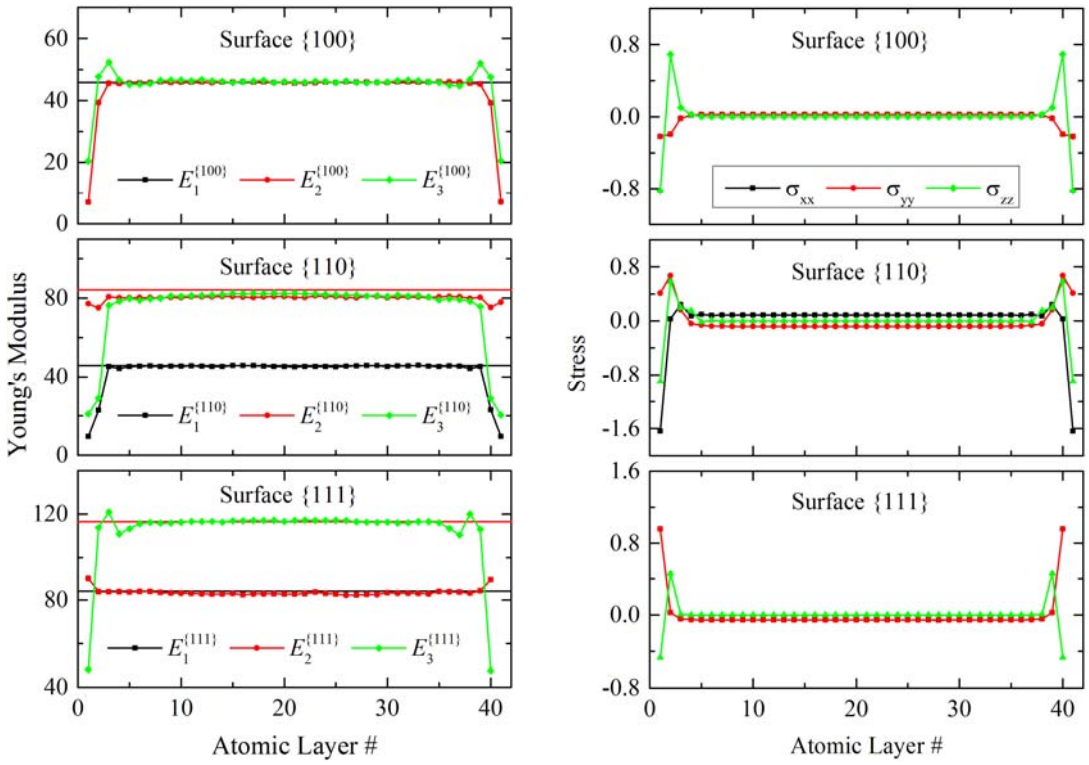


Figure 4 a) Young's moduli for each atomic layer along $Z$ direction for three orthotropic structures with the free surfaces on $\{100\}$, $\{110\}$, and $\{111\}$. Symbols are the results for local elastic constants calculated by Eq. (27), where square, circle, and diamond denote $E_1$, $E_2$ and

$E_3$, respectively. Straight solid lines are the corresponding bulk behavior. b) Average local stress distributions for the three cases.

## 4. Concluding Remarks

In this paper, an explicit and compact form of the estimation of the effective local elasticity tensor is derived from the intermediate modulus and strain concentration tensor, which need to collect the data of local strain, local stress, and global strain. The newly developed approach reduces to the general stress-strain fluctuation formula for the estimation of global moduli when the local variables are replaced by the global ones. Validity and accuracy of the new method is manifested by comparing the local elasticity tensors with bulk behavior for FCC crystalline structures.

As an example to illustrate the application of this new technique, we investigate the free surface effect on the mechanical properties. Our results demonstrate the mechanical heterogeneity for nano-sized structures. A surface may be softer or stiffer than the corresponding bulk behavior, depending on the surface orientations and loading directions. Such phenomena are solely determined by the atomic coordination change on surfaces. It should be noted that the presence of surface stress leads to a non-hydrostatic bulk stress in the bulk regions inside the slab, as observed by small non-zero stresses along $X$ and $Y$ directions in Figure 4 b). Moreover, the magnitudes of these stresses could reduce for a thicker film. Therefore the local moduli of surfaces are size-dependent and should converge for a bulk system.

In closing we need to point out that polymers are not yet considered in this work due to large simulation sizes and appropriate coarse graining potentials. These are the subject of future work. Additionally, a better atomic volume model for the free surface layer will lead to improved

results. Overall, this new approach will be a powerful tool for the modeling and simulation of other inhomogeneous materials, such as the interphase of polymer-based nano-composites [45], interface formed between different crystallographic directions [46], etc. It will enables validation of the various continuum models on the prediction of the effective modulus for heterogeneous materials; the approach can be used to estimate the mechanical performances that are difficult to obtain experimentally; and it will give us a means to explore and compare the roles of polymer-substrate interactions and geometrical constraints on elastic properties.

**Acknowledgements**

This work was performed under the following financial assistance award 70NANB14H012 from U.S. Department of Commerce, National Institute of Standards and Technology as part of the Center for Hierarchical Materials Design (CHiMaD), award N000141410434 from Office of Naval Research, and award FA95501410032 from Air Force Office of Scientific Research. The authors would like to thank Dr. Marc James Palmeri for fruitful discussions.

## Reference


[1] Y. C. Ou, Z. Z. Yu, A. Vidal, and J. B. Donnet, J Appl Polym Sci **59**, 1321 (1996).
[2] A. M. Huang, X. P. Wang, D. M. Jia, and Y. M. Li, E-Polymers **7**, 588 (2007).
[3] H. Yang, M. Tian, Q. X. Jia, J. H. Shi, L. Q. Zhang, S. H. Lim, Z. Z. Yu, and Y. W. Mai, Acta Mater **55**, 6372 (2007).
[4] C. J. Ellison, and J. M. Torkelson, Nature Materials **2**, 695 (2003).
[5] J. A. Forrest, K. DalnokiVeress, and J. R. Dutcher, Physical Review E **56**, 5705 (1997).
[6] S. Watcharotone, C. D. Wood, R. Friedrich, X. Q. Chen, R. Qiao, K. Putz, and L. C. Brinson, Adv Eng Mater **13**, 400 (2011).
[7] K. Van Workum, and J. J. de Pablo, Phys Rev E **67**, 031601 (2003).
[8] K. Yoshimoto, T. S. Jain, K. V. Workum, P. F. Nealey, and J. J. de Pablo, Phys Rev Lett **93**, 175501 (2004).
[9] R. A. Riggleman, J. F. Douglas, and J. J. de Pablo, Soft Matter **6**, 292 (2010).
[10] J. Qu, and M. Cherkaoui, *Fundamentals of Micromechanics of Solids* (John Wiley & Sons, Inc., 2006).
[11] Z. W. Cui, Y. Sun, and J. M. Qu, Mol Simulat **39**, 956 (2013).
[12] Z. W. Cui, Y. Sun, and J. M. Qu, Solid State Ionics **226**, 24 (2012).
[13] S. R. Yang, Z. W. Cui, and J. M. Qu, J Phys Chem B **118**, 1660 (2014).
[14] M. Sprik, R. W. Impey, and M. L. Klein, Phys Rev B **29**, 4368 (1984).
[15] Y. B. Zhen, and C. B. Chu, Comput Phys Commun **183**, 261 (2012).
[16] M. Parrinello, and A. Rahman, J Chem Phys **76**, 2662 (1982).
[17] A. A. Gusev, M. M. Zehnder, and U. W. Suter, Phys Rev B **54**, 1 (1996).
[18] Z. W. Cui, Y. Sun, J. Li, and J. M. Qu, Phys Rev B **75**, 214101 (2007).
[19] J. Li, Y. Sun, Z. W. Cui, and F. L. Zeng, Comput Phys Commun **182**, 1447 (2011).
[20] J. Cormier, J. M. Rickman, and T. J. Delph, J Appl Phys **89**, 99 (2001).
[21] H. Mizuno, S. Mossa, and J. L. Barrat, Phys Rev E **87**, 042306 (2013).
[22] J. R. Ray, and A. Rahman, J Chem Phys **82**, 4243 (1985).
[23] J. R. Ray, and A. Rahman, J Chem Phys **80**, 4423 (1984).
[24] J. R. Ray, M. C. Moody, and A. Rahman, Phys Rev B **32**, 733 (1985).
[25] I. Goldhirsch, and C. Goldenberg, Eur Phys J E **9**, 245 (2002).
[26] G. J. Papakonstantopoulos, K. Yoshimoto, M. Doxastakis, P. F. Nealey, and J. J. de Pablo, Phys Rev E **72**, 031801 (2005).
[27] J. F. Lutsko, J Appl Phys **64**, 1152 (1988).
[28] Z. W. Cui, and L. C. Brinson, Phys Rev E **88**, 022602 (2013).
[29] Q. W. Zheng, J. W. Cui, X. F. Yu, Q. Guo, H. Zhou, and D. Y. Ren, Chinese Phys Lett **31**, 126101 (2014).
[30] Y. H. Wen, Y. Zhang, and Z. Z. Zhu, Phys Rev B **76**, 125423 (2007).
[31] F. Shimizu, S. Ogata, and J. Li, Mater Trans **48**, 2923 (2007).
[32] M. L. Falk, and J. S. Langer, Phys Rev E **57**, 7192 (1998).
[33] S. Plimpton, J Comput Phys **117**, 1 (1995).
[34] http://lammps.sandia.gov/.
[35] G. Cao, and X. Chen, Phys Rev B **76**, 165407 (2007).
[36] P. A. T. Olsson, S. Melin, and C. Persson, Phys Rev B **76**, 224112 (2007).
[37] G. X. Cao, and X. Chen, Int J Solids Struct **45**, 1730 (2008).
[38] J. Hu, X. W. Liu, and B. C. Pan, Nanotechnology **19**, 285710 (2008).
[39] R. Dingreville, J. M. Qu, and M. Cherkaoui, J Mech Phys Solids **53**, 1827 (2005).

[40] P. Lu, L. H. He, H. P. Lee, and C. Lu, Int J Solids Struct **43**, 4631 (2006).
[41] A. R. Khoei, and A. Aramoon, Mat Sci Eng C-Mater **32**, 1993 (2012).
[42] L. G. Zhou, and H. C. Huang, Appl Phys Lett **84**, 1940 (2004).
[43] S. S. Liu, Y. H. Wen, and Z. Z. Zhu, Chinese Phys B **17**, 2621 (2008).
[44] X. Cheng, in *PhD thesis* (Northwestern University, Evanston, IL, 2014).
[45] X. Cheng, K. W. Putz, C. D. Wood, and L. C. Brinson, Macromol Rapid Comm **36**, 391 (2015).
[46] C. Mi, S. Jun, D. A. Kouris, and S. Y. Kim, Phys Rev B **77**, 075425 (2008).